Supplemetary Material and Methods

MALDI-TOF-MS

2 µL of a 9 mg/mL mixture of 2,5-dihydroxybenzoic acid (DHB) in 30% acetonitrile was applied to a MTP 384-spot ground steel target plate TF (Bruker Daltonics). A 1 µL sample was then mixed into the DHB droplet and dried under a stream of air. The samples were analysed with an Ultraflex MALDI-ToF/ToF instrument (Bruker Daltonics GmbH, Bremen, Germany) equipped with a nitrogen 337 nm laser beam. The instrument was operated in positive acquisition mode and controlled by the FlexControl 3.0 software package. All spectra were obtained using the reflectron mode with an acceleration voltage of 25kV, a reflector voltage of 26kV, and pulsed ion extraction of 40 ns in the positive ion mode. The acquisition range used was from *m/z* 0 to 4000. The data was collected from averaging 1000 laser shots, with the lowest laser energy necessary to obtain sufficient signal to noise ratios. Peak lists were generated from the MS spectra using Bruker FlexAnalysis software (Version 3.3).

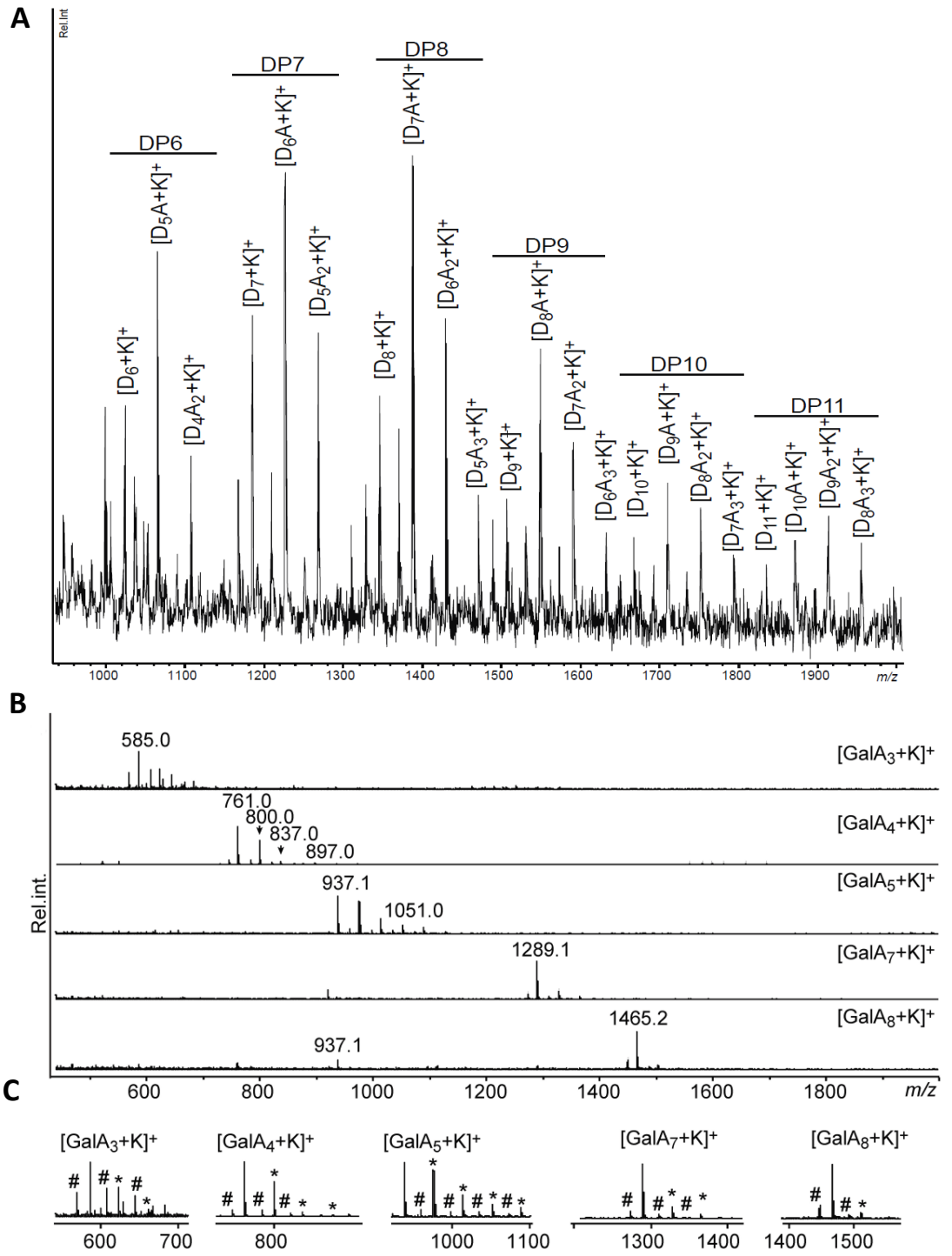

Fig. S1. Oligosaccharide analysis using MALDI-ToF-MS. (A) MALDI-ToF-MS spectrum of the chitosan oligosaccharides used to produce the COS probes. D_n is the degree of polymerisation and A_n is the number N-acetyl substitutions (B) MALDI-ToF-MS spectra of oligogalacturonides used on the microarrays and, in the case of GalA7, used to produce OGA probes. (C) Mass spectrum fragments showing sodium (hash) and potassium (asterisk) adducts from the spectrum shown in (B).

A

Pectins with a range of degrees of methyl esterification (DE)																									
DE 0%	DE 11%	DE 19%	DE 31%	DE 58%	DE 69%	DE 76%	Rhamnogalacturonan I (Potato)	Xyloglucan	(1→3),(1→4)-β-D-glucan	(1→3),(1→4)-β-D-glucan	Methyl cellulose	Pectic arabinan	Pectic galactan	Pectic galactan	Pullulan	Laminarin	Linear Arabinan	Arabinogalactan	Chondroitin sulfate	Galactomannan	Glucomannan	Gum arabic	Gum ghatti	Glucuronoxylan	Chitosan	Partially acetylated chitosan	
18	51	86	86	87	91	75	5	0	0	0	0	0	0	0	0	0	8	0	0	0	0	0	0	0	0	0	JIM5
42	52	59	59	50	56	35	0	0	0	0	0	0	0	0	0	0	0	0	0	0	0	0	0	0	0	0	LM18
57	64	62	53	45	51	25	7	0	0	0	0	0	14	10	0	0	0	0	0	0	0	0	0	0	0	0	LM19
87	100	67	16	0	6	0	14	0	0	0	0	0	0	13	0	0	0	0	0	0	0	0	0	0	0	0	2F4
100	75	8	0	0	0	0	0	0	0	0	0	0	0	0	0	0	0	0	0	0	0	0	0	0	0	0	PAM1
0	0	0	0	20	26	30	0	0	0	0	0	0	0	0	0	0	0	0	0	0	0	0	0	0	0	0	LM20
19	7	37	48	63	65	58	6	0	0	0	0	7	11	11	0	0	11	0	0	0	0	0	0	0	0	0	JIM7
56	60	0	0	0	0	0	0	0	0	0	0	0	0	0	0	0	0	0	0	0	0	0	0	0	0	0	COS^{488}
0	0	0	0	0	0	0	0	0	0	0	0	0	0	0	0	0	0	0	0	0	0	0	0	0	100	41	OGA^{488}

Anti-HG antibodies

Polysaccharides

B

Arabinooctaose α-L-Araf-(1→5)-[α-L-Araf-(1→5)]$_6$-L-Araf	Mannohexaose β-D-Manp-(1→4)-[β-D-Manp-(1→4)]$_4$-D-Manp	Lactose β-D-Glcp-(1→4)-[β-D-Glcp-(1→4)]$_4$-D-Glcp	Xyloglucan heptamer, XXXG*	Xylohexaose β-D-Xylp-(1→4)-[β-D-Xylp-(1→4)]$_4$-D-Xylp	Glucotetraose [G4G3G4G-OH] β-D-Glcp-(1→4)-β-D-Glcp-(1→3)-β-D-Glcp-(1→4)-β-D-Glcp	Laminarihexaose β-D-Glcp-(1→3)-[β-D-Glcp-(1→3)]$_4$-D-Glcp	Maltohexaose α-D-Glcp-(1→4)-[α-D-Glcp-(1→4)]$_4$-D-Glcp	Cellohexaose β-D-Glcp-(1→4)-[β-D-Glcp-(1→4)]$_4$-D-Glcp	Trigalacturonate α-D-GalpA-(1→4)-α-D-GalpA-α-D-GalpA	Tetragalacturonate α-D-GalpA-(1→4)-[α-D-GalpA-(1→4)]$_2$-α-D-GalpA	Pentagalacturonate α-D-GalpA-(1→4)-[α-D-GalpA-(1→4)]$_3$-α-D-GalpA	Heptagalacturonate α-D-GalpA-(1→4)-[α-D-GalpA-(1→4)]$_5$-α-D-GalpA	Octagalacturonate α-D-GalpA-(1→4)-[α-D-GalpA-(1→4)]$_6$-α-D-GalpA	Chitohexaose β-D-GlcpNAc-(1→4)-[β-D-GlcpNAc-(1→4)]$_4$-β-D-GlcpNAc	DNA Salmon sperm	BSA	
0	0	0	0	0	0	11	0	15	0	0	0	0	0	0	0	0	JIM5
0	0	0	0	0	0	0	0	7	0	0	0	6	22	5	0	0	LM18
0	0	0	0	0	0	0	0	6	0	0	0	32	49	0	0	0	LM19
0	0	0	0	0	0	0	0	0	0	0	0	0	0	9	0	0	2F4
0	0	0	0	0	0	0	0	0	0	0	0	0	0	0	62	0	PAM1
0	0	0	0	0	0	0	0	0	0	0	0	0	0	0	0	0	LM20
0	0	0	0	0	0	7	6	7	0	0	0	0	0	0	0	0	JIM7
0	0	0	0	0	0	0	0	0	0	0	13	35	77	0	7	0	COS^{488}
0	0	0	0	0	0	0	0	0	0	0	0	0	0	0	0	0	OGA^{488}

Anti-HG antibodies

Oligosaccharides

C

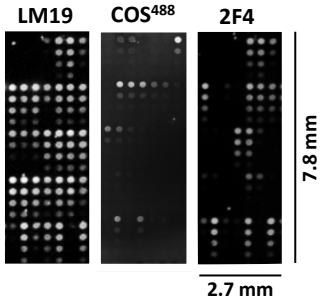

Fig. S2. Binding specificity of COS and OGA. Carbohydrate microarrays populated with (A) polysaccharides and (B) oligosaccharides were probed with a selection of anti-homogalacturonan antibodies (listed to the right), COS^{488} and OGA^{488}. The heatmap shows mean signal intensities from three replicate arrays. The highest signal in the data set was set to 100 and all other values adjusted accordingly. (C) Representative examples of carbohydrate microarrays from which the heatmap was produced.

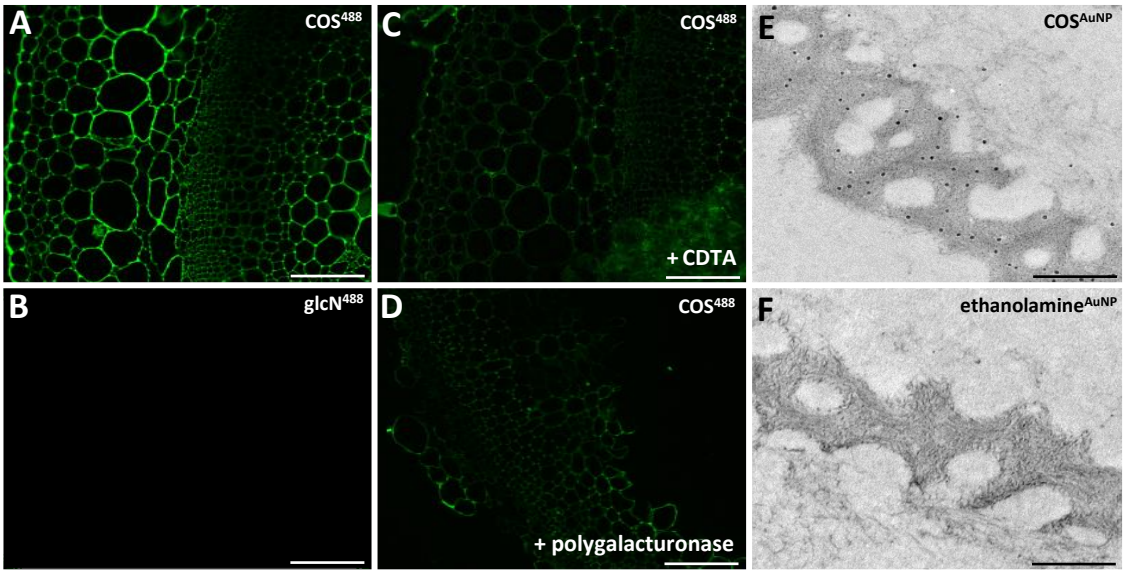

Fig. S3. Microscopy labelling controls for COS binding. (A-D) Sections through tobacco stem labelled with COS^{488} (A) and control conjugate $glucosamine^{488}$ (B). Glucosamine was coupled to Alexa Fluor 488 using the same procedure as for COS^{488}. Binding of COS^{488} to tobacco sections was reduced by pre-treatment with a reagent used to extract pectins 1,2-cyclohexanediaminetetraaceticacid (C) and the homogalacturonan-degrading enzyme polygalacturonase (D). (E) Transmission electron microscopy images showing resin-embedded sections of *P. margaritaceum* labelled with COS coupled with nanogold particles (COS^{AuNP}) and enhanced with silver. (F) A control image showing labelling with $ethanolamine^{AuNP}$. Scale bars: 100 μm for A-D; 1 μm for E,F.

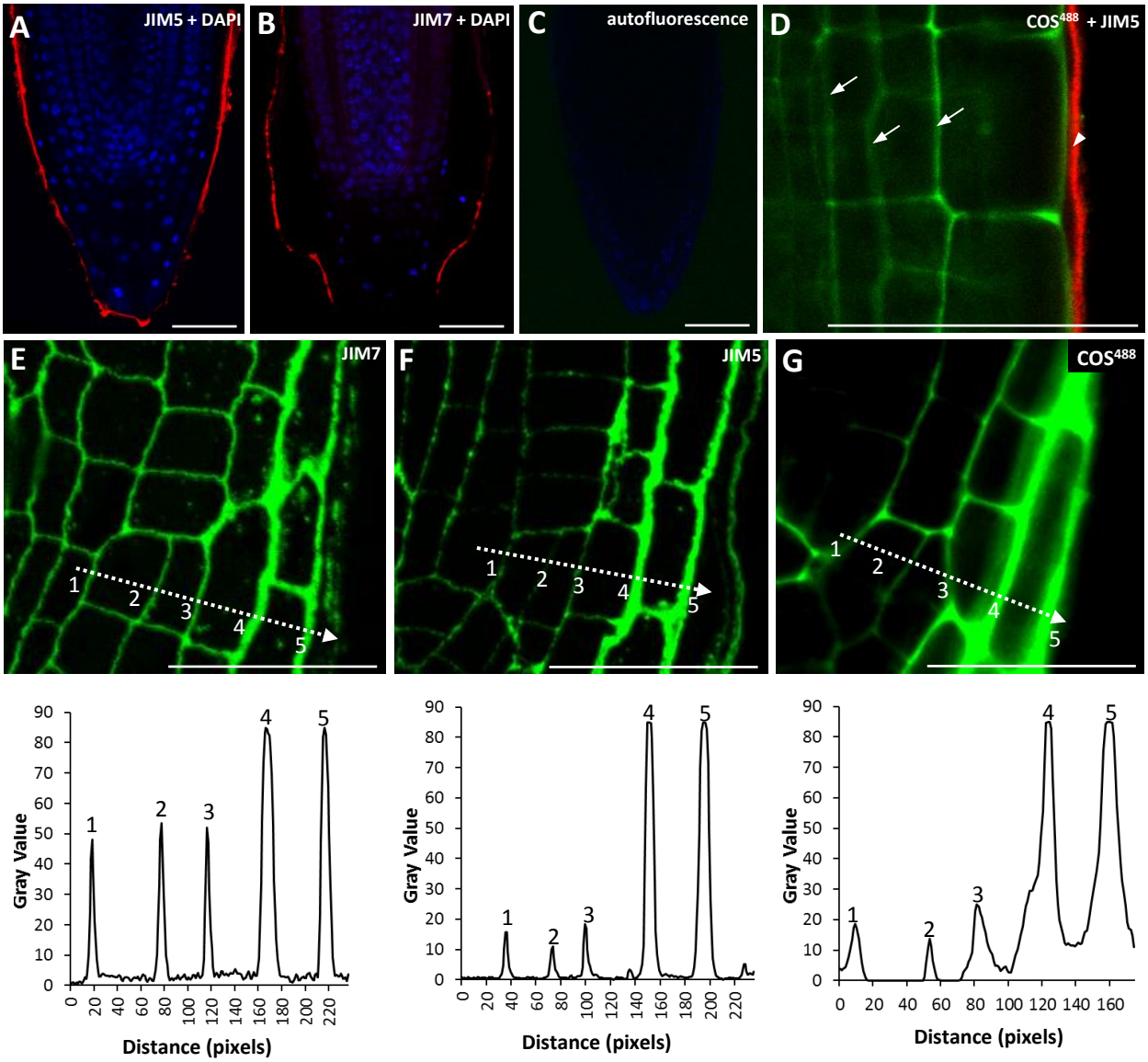

Fig. S4. Analyses of root tip labelling by mAbs and COS probes. (A,B) Whole mount labelling of *Arabidopsis* root tips using JIM5 (A) and JIM7 (B). Antibody binding was visualized using with rhodamine-tagged secondary antibody (red). Nuclei are stained with DAPI blue. (C) Control image showing an *Arabidopsis* root tip labeled with secondary antibody only. (D) Dual labelling of a whole unfixed *Arabidopsis* root with COS^{488} (green) and the anti-HG monoclonal antibody JIM5 (detected with rhodamine-tagged secondary antibody, red). Note that whilst COS^{488} penetrates to the cortical parenchyma (arrows), JIM5 does not penetrate the root (arrowhead). (E-G) Signal intensity analyses of HG labelling in lateral root caps. (E,F) Top panels, sections through resin-embedded root tips labeled by antibodies (E) JIM7 and (F) JIM5. (G) *In vivo* labeling of a whole root tip using COS^{488}. Bottom panels: plot profiles showing fluorescence intensities of the regions indicated by the dashed line in the panels above. The positions of the areas producing the peaks are indicated by numbers 1-5. Note that the signal plot profiles indicate a significant increase of JIM5 and COS^{488} labelling in the mature root cap layers (4 and 5) compared to antibody JIM7. Scale bars: 10 μm

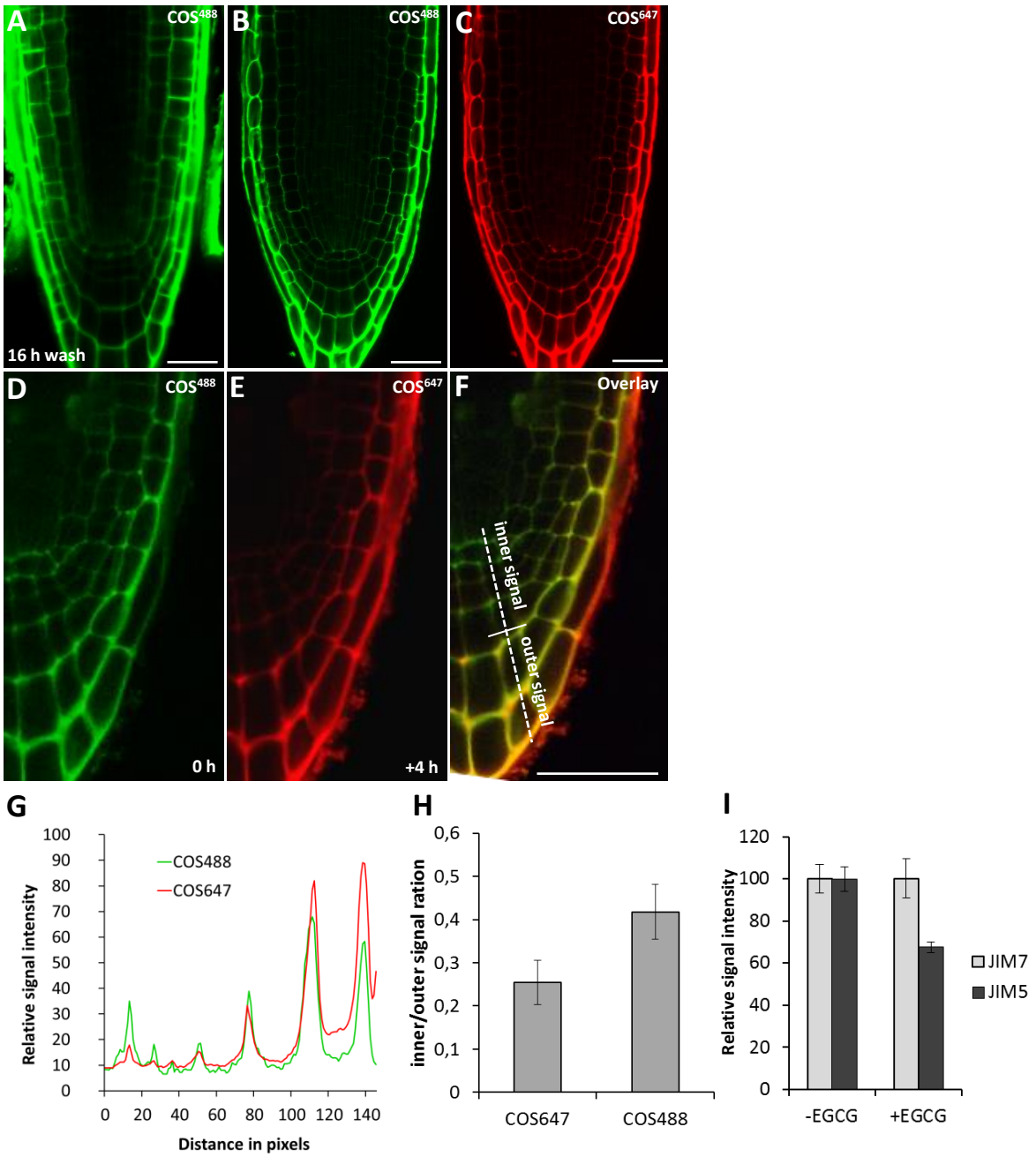

Fig. S5. Dynamics of HG turn-over in root cap. (A) Control for the stability of the COS^{488} labelling. Fixed roots were stained with COS^{488}, washed 3 times and incubated in the labelling buffer for 16h before scanning. No significant wash-out of the probe was observed. (B,C) Comparison of two COS fluorescent variants simultaneously applied to root tips. (B) COS^{488} and (C) COS^{647} have identical labeling patterns and penetration properties. (D-G) Time lapse labeling of the root tip by two COS variants but in a reverse order as shown in Fig. 3H-K. Seedlings were labelled first using COS^{488}, washed and allowed to grow for 4 hours. Seedlings were then re-labelled with COS^{647} and washed. The simultaneous scan of (D) COS^{488} and (E) COS^{647} labelling at the end of the experiment. (F) Overlay image showing the occurrence of newly formed epitopes present in mature layers of the root tip. (G) Plot profile of the dashed line indicated in (F). (H) Quantification of the difference in signal intensities from COS^{488} and COS^{647} in the 'inner' and 'outer' regions indicted in (F) from 8 root tips. The inner region denotes the first three columella layers and outer region the last two columella layers. Note the higher difference between the two signals in the case of COS^{647} (freshly formed epitopes) labelling indicating more signal from the outer region. (I) The effect of EGCG (4 hours at 200 μM EGCG) on JIM5 and JIM7 labeling of root tip resin sections. The JIM7 signal was unchanged whilst the JIM5 signal was reduced in roots treated by EGCG. Error bars indicate s.e.m. n=8. Scale bars: 10 μm

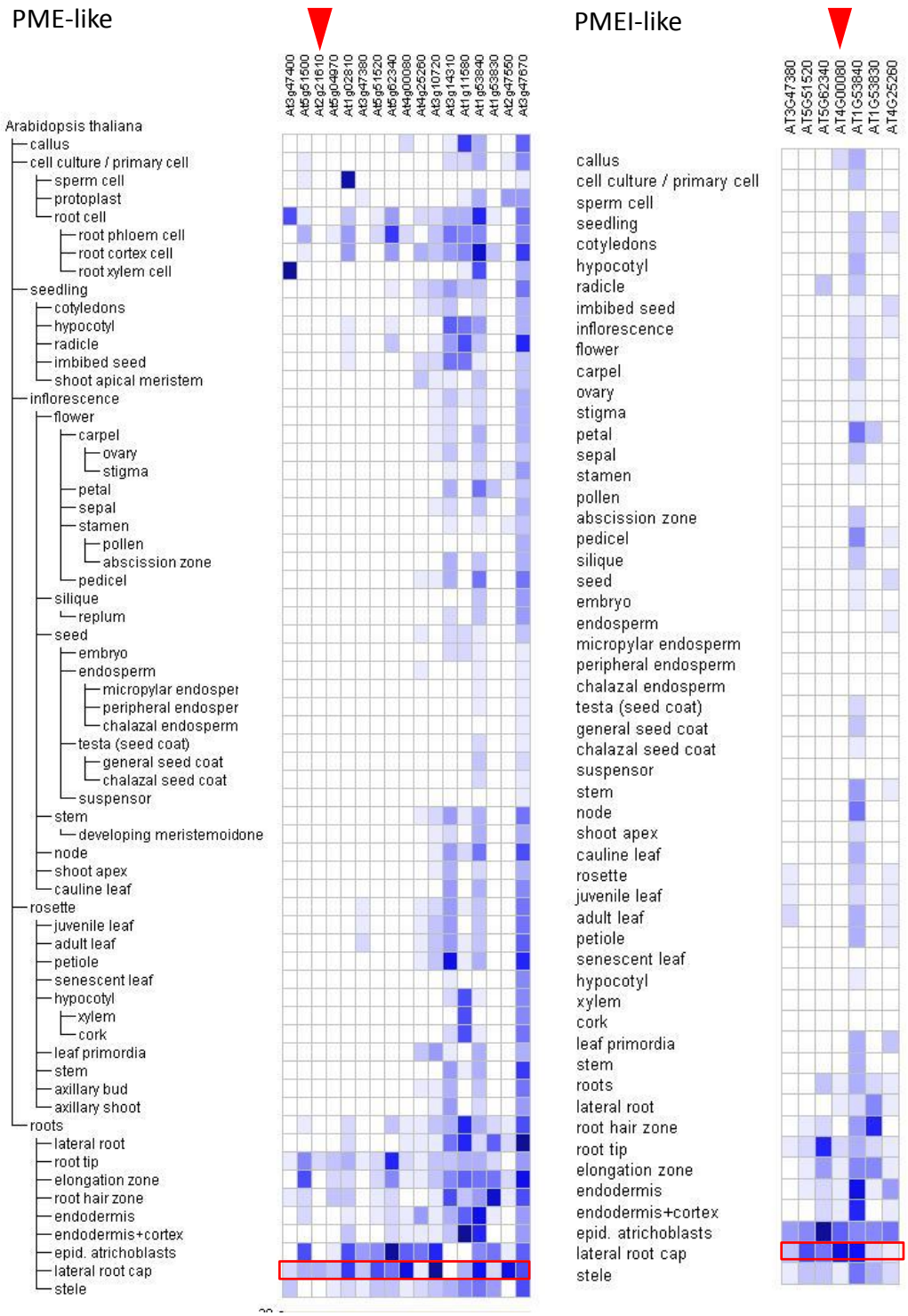

Fig. S6. *In silico* expression analyses of PME- and PME-like genes. Microarray data of PME-like and PMEI-like genes expressed in *Arabidopsis* root tip from public database (https://www.genevestigator.com). Only those with significant expression in root tips are shown. The expression in the root cap is highlighted by red outline. The root cap specific genes analyzed by GUS reporter constructs are indicated by red arrowheads.

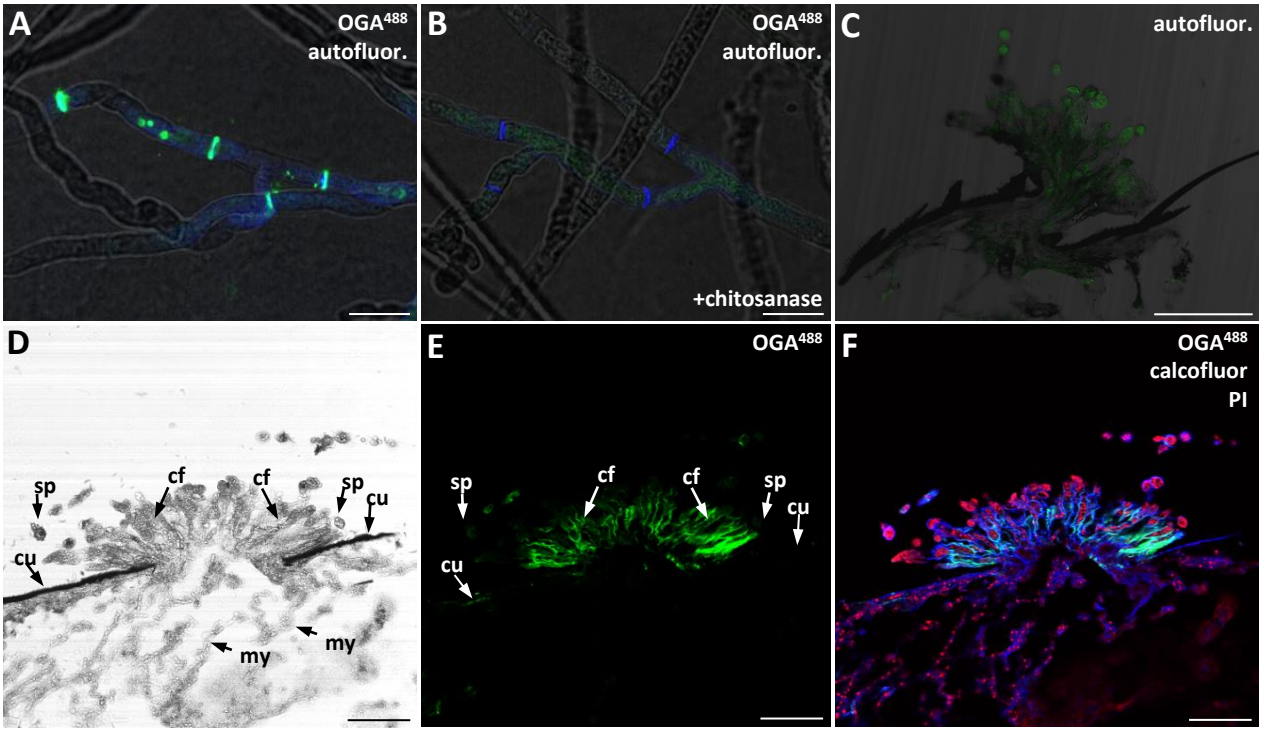

Fig. S7. Microscopy labelling controls for OGA^{488} in fungi. (A,B) Chitosanase treatment removes the OGA^{488} signal (green) in *Neurospora crassa.* Images are overlays with bright field and autofluorescence (blue). (A) Labeling of *N. crassa* mycelium by OGA^{488}. (B) Labeling by OGA4^{88} after chitosanase treatment showing decrease in signal. (C) Control image of unlabeled *E. scizhophorae.* (D) Bright field image of a section through *M. domestica* abdomen infected with *E. scizhophorae*. Conidiophores (cf) and spores (sp) can be seen emerging through the membrane between two cuticle (cu) plates. Hyphae in the mycelia (my) can be seen inside the abdomen. (E) Image shows the same section as in (D) labelled with OGA^{488} (green) to reveal chitosan. Note that conidiophores are strongly labelled but not the mycelia or spores. (F) Image showing the same section as in (D) but triple labelled with OGA^{488} (green), calcofluor (blue) to reveal chitin and propidium iodide (red) to show nucleic acids. Scale bars: 10 μm

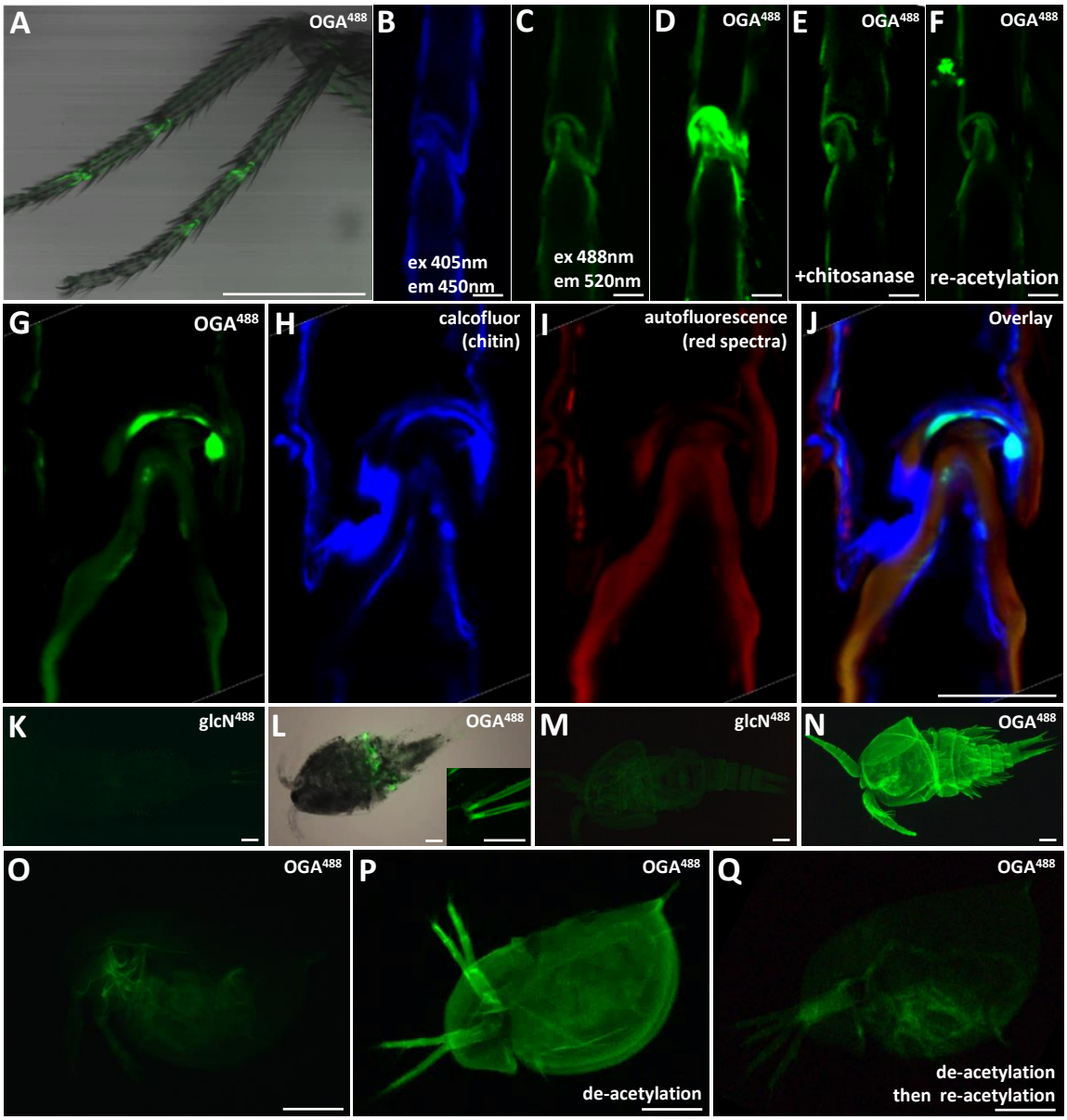

Fig. S8. Microscopy labelling controls for OGA^{488} in arthropods. (A) Labeling of a whole *Drosophila* leg using OGA^{488}. Note the labelling in the tarsal joints. (B-F) Labeling controls for OGA^{488} in *Drosophila* joints. (B) Unlabeled control with excitation at 305 nm and emission at 450 nm. (C) Unlabeled control with excitation at 488 nm and emission at 520 nm. (D) Labeling with OGA^{488}. Note the strong labelling in the tarsal joint. (E) Chitosanase treatment and (F) chemical re-acetylation of NaOH-treated samples severely decreases OGA^{488} binding. (G-J) Labeling of thin resin sections of *Drosophila* tarsal joints. (G) OGA^{488} signal. (H) Calcofluor labelling of chitin. (I) Autofluorescence signal with excitation at 555 nm and emission at 620 nm. (J) Overlay of the three channels from (G), (H) and (I). Note the partial co-localization of OGA^{488} and calcofluor labelling. (K-N) Labeling of *Cyclops sp.* (K,L) Labelling of untreated *Cyclops sp*. with (K) control conjugate glucosamine^{488} and (L) OGA^{488}. The picture is an overlay of bright field and the 488 nm channel. Note the central region and the tail labelling (inset). (M, N) Labelling of *Cyclops* sp. after pre-treatment by 5M sodium hydroxide at 99 °C for 1 hour (chemical de-acetylation) by (M) control glucosamine^{488} and (N) OGA^{488}. The whole exoskeleton containing chemically de-acetylated chitin is visible. (O-R) Labeling of *Dafnia pulex* acetylation control. (O) Labeling of the untreated *Dafnia.* (P) Labeling of chemically de-acetylated *Dafnia.* The whole exoskeleton is visible.(Q) When de-acetylated *Dafnia* was again chemically re-acetylated no signal is visible after OGA^{488} labelling. Scale bars: 10 μm for B-J; 100 μm for A and K-Q.